NUMERICAL SIMULATION OF GOLD NANOSTRUCTURE ABSORPTION EFFICIENCY FOR FIBER-OPTIC PHOTOACOUSTIC GENERATION

Ye Tian[1], Hamzeh Jaradat[1], Nan Wu[1], Xiaotian Zou[2], Yang Zhang[1], Yuqian Liu[3], Alkim Akyurtlu[1], Chengyu Cao[3], and Xingwei Wang[1, *]

[1]Department of Electrical and Computer Engineering, University of Massachusetts Lowell, One University Ave., Lowell, MA 01854, USA

[2]Department of Biomedical Engineering and Biotechnology, University of Massachusetts Lowell, One University Ave., Lowell, MA 01854, USA

[3]Department of Mechanical Engineering, University of Connecticut, Storrs, CT 06269, USA

Abstract—In many non-destructive testing and medical diagnostic applications, photoacoustic generation by optical fiber is an effective approach to meet the requirements of broad bandwidth and compact size. The energy absorption layer coated onto the fiber endface plays an important role in the conversion of laser energy into heat used to excite acoustic waves. Gold nanostructures are promising solutions to be utilized as energy absorption layers due to their capability of absorbing maximum optical energy at plasmon resonant frequencies. The appropriate selection of the organization and dimensions of the gold nanostructures is the key to achieving high absorption efficiency. Numerical modeling is an efficient way to predict the behavior of the system as a variation of select parameters. A 3D finite integral technique model was established to simulate the dependency of absorption efficiency on the organization and dimensions of the gold nanospheres and nanorods. The simulation results provided practical clues to the design and fabrication of fiber-optic photoacoustic generators.

* Corresponding author: Xingwei Wang (xingwei_wang@uml.edu).

1. INTRODUCTION

A multitude of ultrasound transducers has been developed for non-destructive testing in a variety of applications [1, 2]. Compared to traditional ultrasound generators [3], optical ultrasound generators, especially fiber-optic ultrasound generators, are more suitable for high-quality testing applications found inside confined spaces, due to their pertinent advantages such as compact size, electromagnetic interference immunity (EMI), and wide bandwidth [4, 5]. The core operating mechanism in the optical approach is based on photoacoustic principles, in which pulsed optical energy is converted into heat that generates ultrasound pulses by an energy absorption layer [6].

Both the coefficient of thermal expansion (CTE) and optical energy absorption capability of the photoacoustic element are critical to the photoacoustic generation efficiency [7, 8]. It has been demonstrated that epoxy, or Polydimethylsiloxane (PDMS), along with photo-absorptive materials, could serve as a high CTE material for high photoacoustic generation efficiency [6, 9]. The optical absorption coefficient of the photo-absorptive material at the operating laser wavelength can be further increased. The focus of this paper is to simulate the dependency of absorption efficiency on the organization and dimensions of the photo-absorptive material. Gold nanoparticles exhibit maximum optical energy absorption at the wavelength around 520 nm when the diameter is 20 to 50 nm [10]. It has also been experimentally observed that various gold nanostructures are good absorption materials due to the high optical energy absorption behavior occurring at their plasmon resonant frequency [11–13]. Compared to random gold nanostructures, periodic gold nanostructures have higher absorption efficiency because of the increased interaction time by the localized surface plasmon [14]. Recently, focused ion beam (FIB) is available to directly fabricate the periodic gold nanostructures on the fiber endface [15, 16]. However, it is still not clear how the absorption efficiency is affected by the organization, dimensions, and spacing of the gold nanostructures.

Many methods have been used to model the optical properties of gold nanostructures. Mie theory provides a good method of analyzing the optical absorption spectrum of a single spherical nanoparticle of arbitrary size [17]. However, by ignoring the dielectric factors, size, and shape of the nanostructures, Mie theory is not sufficient to provide accurate results [18, 19]. Discrete dipole approximation (DDA) method is another powerful method of characterizing the optical properties of gold nanostructures for arbitrary shapes and sizes in an asymmetric environment [20]. Nevertheless, its main

disadvantage is that it is not able to calculate extended and periodic structures [21]. Similarly, finite-difference time domain (FDTD) method is able to characterize gold nanostructures in a dielectric environment by using a non-uniform grid to calculate the absorption and scattering properties [22, 23]. Unfortunately, this method ignores the coupling effect between adjacent spherical nanoparticles. Finally, finite integral technique (FIT) with an integral form is highly accurate for simulating periodic nanostructures in both time and frequency domain [24, 25].

This paper presents a 3D FIT model of gold nanostructures used to predict the absorption efficiency of energy absorption materials that are dependent on select physical parameters. The simulation demonstrated that the shape, diameter, organization, separation, layer number, and refractive index of the environment surrounding the gold nanostructure affect the absorption efficiency. The results from this model may be used as a guide in the design and fabrication of fiber-optic photoacoustic generators.

2. METHOD

The dielectric fiber mainly serves for the purpose of light transmission. We are using single mode fibers and focusing on how much light from the fiber can be absorbed, so the high order modes do not affect the photoacoustic generation. It is expected that most of the transmitted light will be absorbed by the gold nanopatterns on the fiber endface. However, the refractive index difference between the fiber and the surrounding medium affects the interface reflection, subsequently the absorption efficiency. Therefore, refractive indexes of the materials, as the major optical property, will be taken into consideration in the simulation. The optical fiber core was modeled as a lossless dielectric material with a homogenous refractive index of 1.46. The gold nanopatterns on the fiber endface are important for light energy absorption. So this modeling is specific to the optical absorption efficiency of the gold nanopattern on the fiber endface. Generally, the nanofabrication on an optical fiber, as seen in focused ion beam, is expensive. It is valuable to have some simulation predictions about how the absorption efficiency will be affected by the organization, dimensions, and spacing of the gold nanostructures before the nanofabrication. The dispersion function for the gold nanostructures was loaded from the experimental data results obtained from the literatures [26–28]. Gold nanoparticles exhibit maximum optical energy absorption at the wavelength around 520 nm when the diameter is 20 to 50 nm [10]. A laser with a wavelength of around

520 nm was used in the experiment, so the absorption peak around 520 nm was expected in the simulation. In this paper, the absorption efficiency at the peak wavelength as well as at two typical wavelengths 430 nm and 700 nm away from the peak wavelength were compared. A series of simulations was performed to observe the absorption efficiency of single-layered gold nanospheres with different distributions. Then, multi-layered patterns with different filling material were simulated to further improve the absorption efficiency. Finally, a simpler pattern of single-layered nanorods was simulated to find the optimized diameter, separation, and height.

All results presented in this work were obtained by using the well-established 3D electromagnetic simulator computer simulation technology (CST) [29], specifically CST microwave studio (CST MWS), which is a high-frequency solver package based on the FIT. This package contains an application called the frequency domain (FD) solver, which is highly accurate and thus widely used in simulating periodic structures, photonic band gaps (PBGs), for example, frequency selective surfaces (FSSs), and electromagnetic metamaterials (MTMs) structures. A single-unit cell, which consists of a gold sphere setting over a dielectric brick, was considered in all simulations. Materials used are either loaded from the CST material library or imported from a user defined list, for cases in which the data is frequency dependent. Unit cell boundary conditions were chosen in the FD solver in both the x- and y-directions; this step was necessary in order to account for an infinite number of cells in the x-y plane. Open floquet ports were used at $Z_{\min}$ and $Z_{\max}$, where perfectly matched layer (PML) terminated the ports at both ends. From the floquet port setting, only one mode was selected to be excited in the structure. Different Gaussian excitation source signals were used at the $Z_{\min}$ port. Tetrahedral meshing was applied in order to extract the reflection and transmission coefficients, as well as the electric field distributions. The precision of the simulation depended on the structure's mesh density and the frequency samples. Both number of meshes and frequency samples were chosen properly to produce curves that converge to specific response and any further increment wouldn't change the response significantly. In all simulations, almost 30,000 meshes and 1,000 frequency samples were considered. The electric field component of the incident light was aligned to the y-direction, and the magnetic field component of the incident light was aligned to the x-direction. E-field and H-field monitors were utilized to record the field distribution at the desired wavelengths.

3. RESULTS AND DISCUSSION

3.1. Single-layer Nanospheres

A series of simulations was performed to observe the absorption efficiency of single-layered gold nanospheres. As shown in Fig. 1, the gold nanospheres were positioned on the endface of an optical fiber with a refractive index of 1.46. Each spherical gold nanoparticle was surrounded by four other gold nanospheres. A light beam was emitted from the fiber endface onto the nanospheres.

The diameter of the nanospheres was 50 nm and the distance between two nanospheres (center-to-center distance) of the nanostructure, or the lattice constant, was sampled between 75 nm to 260 nm (separation distance of 25 nm to 210 nm). The absorption spectra as a function of the incident wavelength are shown in Fig. 2. The absorption peak occurred at the resonant wavelength of 516 nm. At larger lattice constants, the coupling between the nanospheres was weak and; therefore, the absorption was poorer. At shorter lattice constants, the
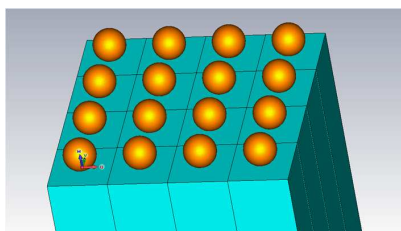

Figure 1. Single-layered gold nanospheres distribution with four neighbor nanospheres.
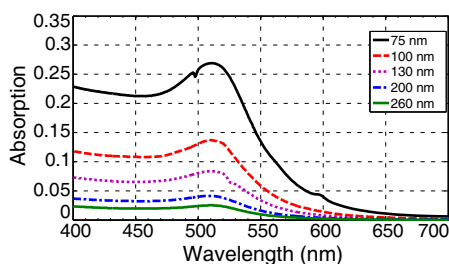

Figure 2. Absorption spectra of single-layered pattern with four neighbor nanospheres. The diameter of the nanospheres was 50 nm and the center-to-center distance of the nanostructure was sampled between 75 nm to 260 nm.

nanostructure became more energy-absorbent due to the increased coupling between the nanospheres. From this observation, the separation distance between the gold nanospheres should be less than 25 nm in order to obtain the highest absorption efficiency.

Moreover, even at a separation distance of less than 25 nm the absorption efficiency of the nanostructure was less than 30%, as illustrated in Fig. 2. It was assumed that if the center nanosphere faced more adjacent nanospheres, then the coupling and also the absorption efficiency would increase. Therefore, another pattern, in which each nanosphere faced six neighbor nanospheres, was simulated to observe the absorption spectra, as shown in Fig. 3.

The nanospheres diameter was fixed at 50 nm, and the lattice constant varied between 75 nm to 260 nm. The absorption spectra as a function of incident wavelength are shown in Fig. 4. Compared to the peak absorption efficiency for the planar cubic pattern, as shown in Fig. 2, the peak absorption efficiency for the closer packed hexagonal
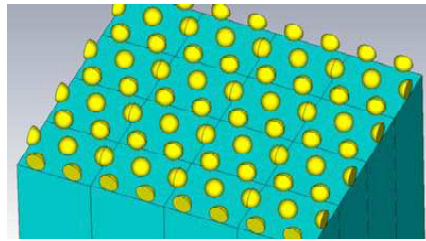

Figure 3. Single-layered gold nanospheres distribution with six neighbor nanospheres.
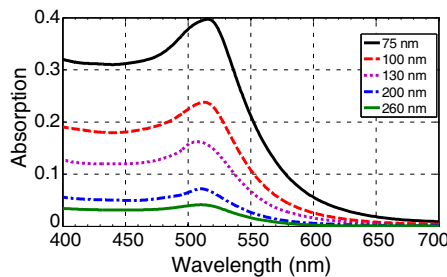

Figure 4. Absorption spectra of single-layered pattern with six neighbor nanospheres. The diameter of the nanoparticlespheres was 50 nm, and the center-to-center distance of the nanostructure was sampled between 75 nm to 260 nm.

pattern increased by more than 50%.

In order to understand the absorption mechanism of the gold nanostructure, the electric, magnetic, and power field distributions were studied. Fig. 5(a) shows the electric field distribution in the y-direction (E_y), magnetic field distribution in the x-direction (H_x), and power distribution in the z-direction (P_z), all evaluated at the resonant wavelength of 516 nm. For the electric field component E_y, the field strength was significantly enhanced at the metal-dielectric interface. The electric field induces positive and negative charges at both ends of the aligned nanospheres. The accumulated charges produce a strong dipole moment along the y-direction through the polarized nanospheres, thereby exciting the surface plasmon resonance (SPR). The magnetic field distribution H_x also showed a strong magnetic field component at resonance. The combined strength of the electric and magnetic resonances force the incident power to be trapped inside
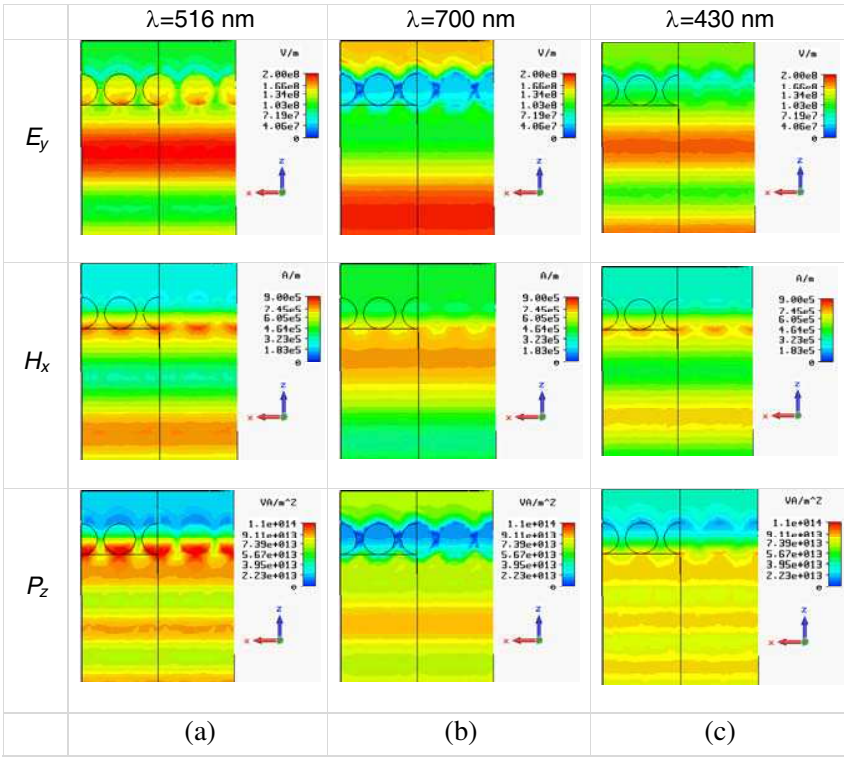

Figure 5. Field distributions for E_y, H_x, and P_z at wavelengths (a) 516 nm, (b) 700 nm, and (c) 430 nm respectively.

the structure and converted into ohmic and dielectric losses. As
seen in the power distribution P_z displayed in Fig. 5(a), the power
was concentrated on the lower side of the nanospheres and dielectric
material. At other incident wavelengths, all the field distributions were
unremarkably weak, as shown in Fig. 5(b) and Fig. 5(c) for incident
wavelengths of 700 nm and 430 nm respectively.

3.2. Multi-layer Nanospheres

As previously demonstrated for the single-layered pattern, higher
absorption efficiency may be achieved by increasing the number of
adjacent nanospheres per unit cell. A multi-layered pattern was
designed to further improve the absorption efficiency, as shown in
Fig. 6. The thickness of each layer was equal to the lattice constant
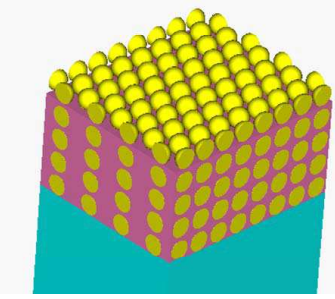for a single layer.

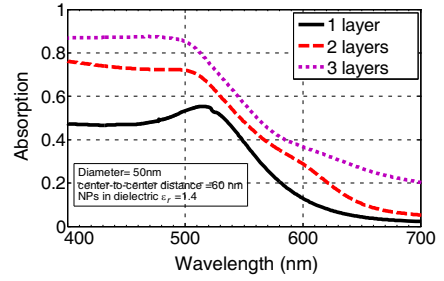**Figure 6.** Multi-layered gold nanospheres distribution.

Figure 7. Absorption spectra of multi-layered pattern with the filling material as a refractive index of 1.4.

In the multi-layered pattern, the 50 nm diameter of the spherical
nanospheres and hexagonal pattern remained fixed while the lattice
constant was changed to 60 nm, and the entire nanostructure was held
together by a polymer filling (refractive index: 1.4). Fig. 7 shows the
absorption spectra of one-, two-, and three-layered patterns. The three-
layered pattern had the highest absorption efficiency of approximately
90%.

In addition, since the dielectric environment changes with filling
material, the influence from this filling parameter was also considered.
As shown in Fig. 8, there was a red shift in the absorption spectra
when the refractive index of the filling material was changed from
1.4 to 1 while the maximum absorption efficiency remained relatively
constant. However, when the refractive index was increased from 1.4
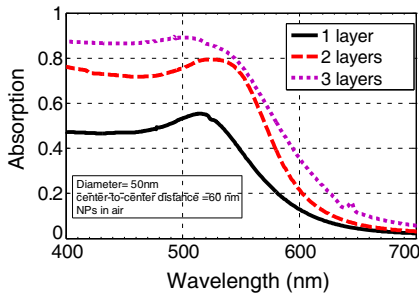
Figure 8. Absorption spectra of multi-layered nanosphere pattern with the filling material as a refractive index of 1.
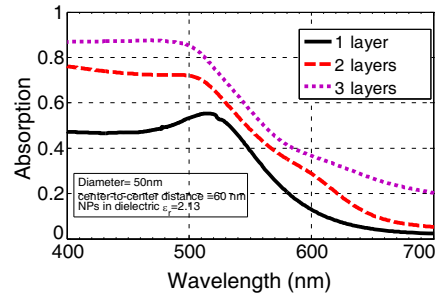
Figure 9. Absorption spectra of multi-layered nanosphere pattern with the filling material as a refractive index of 2.13.

to 2.13, there was no significant difference in the absorption spectra, as shown in Fig. 9. In each case, the absorption efficiency of the multi-layered pattern at a single wavelength (typically 516 nm) was higher than that of the single-layered pattern. This means the multi-layered structure is preferred over the photoacoustic generator operating at a single wavelength. However, the different directions of the peak wavelength shift indicate the effect of the refractive index of the filling material on the peak position. A simpler nanostructure preventing multiple layers is suggested.

Figure 10 shows the peak absorption as a function of the number of layers for each refractive index: 1, 1.4, and 2.13. The trends of the two cases of 1.4 and 2.13 are close. In all cases, when the gold nanostructure was increased from one to three layers the peak absorption increased. However, the peak absorption curve leveled off to approximately 90% in all cases when the gold nanostructure accumulated past three layers. According to the results, 3 layers may be a good choice if the economy of the fabrication is considered. In addition, we are trying to make the absorbing layer as thin as possible to prevent the attenuation of the generated high frequency acoustic signal.

3.3. Nanorods

As demonstrated previously, the absorption efficiency of the gold nanostructure can be largely improved by using multi-layered patterns. This suggests that thicker absorption layers lead to higher absorption efficiency. However, layered structures are not easy to fabricate for real photoacoustic experiments, and too many variables including nanosphere size, center-to-center distance, layer property and layer
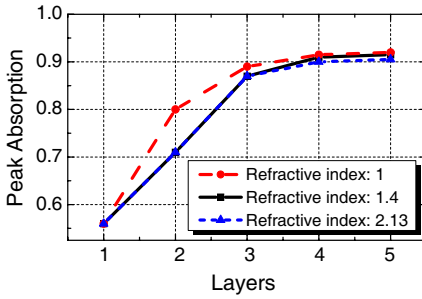
Figure 10. Peak absorption of multi-layer patterns with various filling materials as different refractive indices: 1, 1.4, and 2.13.
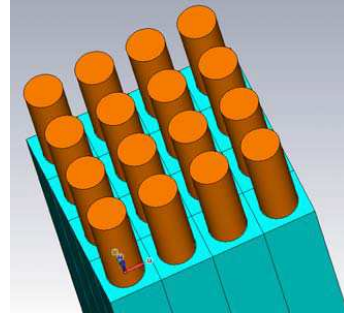
Figure 11. Layout of simple cubic pattern for gold nanorods on top of fiber endface.

thickness make the simulation complicated. A simpler nanostructure preventing multiple layers is suggested. Single-layered nanorods with sufficiently tall heights may be an alternative pattern as they are much easier to fabricate and only consist of three parameters. To simulate this approach, gold nanorods, used as the photoacoustic generation medium, were attached onto the endface of a fiber. The simulation layout is shown in Fig. 11.

The diameter of the nanorods was the first parameter to be analyzed as an independent variable to the absorption spectra. The nanorods had a height of 20 nm, a separation distance (surface-to-surface distance) of 20 nm, and varying diameters ranging from 30 nm to 60 nm. As shown in Fig. 12, the peak absorption observed a slight redshift from 565 nm to 580 nm that coincided with peak absorption coefficients ranging from 0.41 to 0.59. The peak absorption coefficient approached its maximum value when the diameter of the nanorods was approximately 50 nm, as shown in Fig. 13. While holding the diameter constant at 50 nm, other physical parameters, such as the height and separation distance of the nanorods, were observed for maximum energy absorption.

As shown in Fig. 14, the absorption spectra varied as a function of separation distance, while the diameter and height were held constant at 50 nm and 20 nm, respectively. The wavelength of the absorption peak, which is dependent only on the physical dimensions of the nanorods, was approximately 575 nm.

As shown in Fig. 15, when the separation distance was increased from 5 nm to 40 nm, the peak absorption efficiency ranged from 0.48 to 0.58. The peak absorption efficiency approached its maximum value
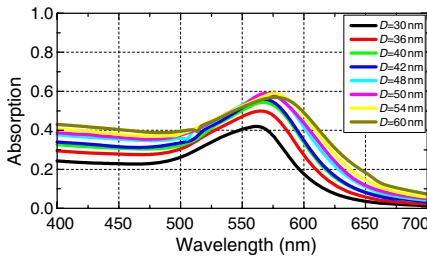
Figure 12. Absorption spectra of gold nanorods by varying diameter (D) from 30 nm to 60 nm at a constant height of 20 nm and separation of 20 nm.
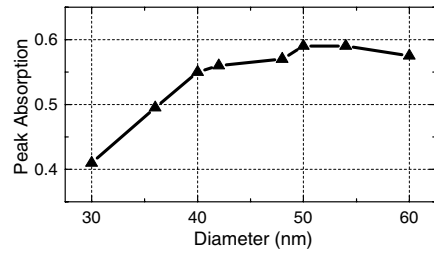
Figure 13. Peak absorption coefficients of gold nanorods by varying diameter from 30 nm to 60 nm at a constant height of 20 nm and separation of 20 nm.
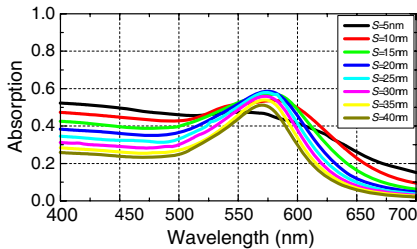
Figure 14. Absorption spectra of gold nanorods by varying separation (S) distance from 5 nm to 40 nm at a diameter of 50 nm and height of 20 nm.
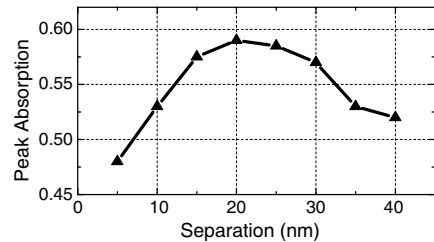
Figure 15. Peak absorption coefficients of gold nanorods by varying separation distance from 5 nm to 40 nm at a constant diameter of 50 nm and height of 20 nm.

when the separation was 20 nm.

The absorption efficiency as a function of height was simulated by holding the diameter and separation distance at 50 nm and 20 nm, respectively, while varying the height, as shown in Fig. 16. From inspection, as the physical dimension was altered, the wavelength of the absorption peak and the magnitude of the absorption efficiency were also altered. In Fig. 17, the peak absorption spectrum decreased between heights of 15 nm and 50 nm, and increased from a height of 50 nm onward. Based on these observations, sufficiently tall, single-layered nanorods may be an alternative pattern for photoacoustic generation instead of the previously demonstrated multi-layered nanostructures. A significant advantage to this pattern is a simpler
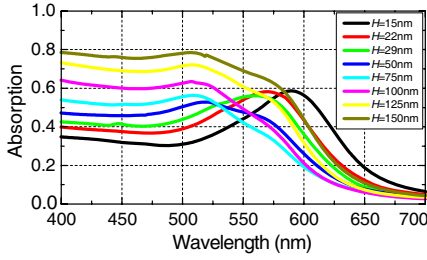
Figure 16. Peak absorption coefficients of gold nanorods by varying height (H) from 15 nm to 150 nm at a constant diameter of 50 nm and separation distance of 20 nm.
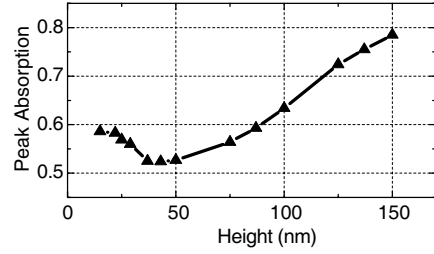
Figure 17. Peak absorption coefficients of gold nanorods by varying height from 15 nm to 150 nm at a constant diameter of 50 nm and separation distance of 20 nm.

fabrication method, and thus reduced manufacturing costs. It is noted that, due to the fast attenuation of high frequency components as the ultrasound propagates along the material, the nanostructures do not need to be as thick as possible. The ideal nanostructure for the photoacoustic application is a high-density periodic gold nanopattern, with a thin thickness that absorbs a sufficient amount of light energy. The absorption efficiency does not need to be 1, but rather 80%–90%, in which cases the thickness of the nanorods is typically 150 nm.

4. CONCLUSIONS

As good energy absorption materials, periodic gold nanostructures can be fabricated onto fiber endfaces for high-efficiency ultrasound generation. A 3D FIT model was established to simulate how the shape, diameter, organization, separation distance, layer number, and refractive index of the environment surrounding the gold nanostructure affect the absorption efficiency. For single-layered gold nanospheres with a diameter of 50 nm, the separation distance between adjacent nanospheres should be less than 25 nm, and more neighbor nanospheres per cell should exist for higher absorption efficiency. Compared to the single-layered nanospheres, the three-layered pattern had much higher absorption efficiency with a maximum absorption efficiency that was close to 90%. For more layers, the efficiency does not increase appreciably due to the saturation of the absorption spectrum. There was also no obvious difference between peak absorption efficiencies when the refractive index of the filling material was varied from 1 to 2.13. Single-layered nanorods that are sufficiently tall may be an

alternative pattern considering their ease of fabrication. The peak absorption efficiency of a nanorod pattern that is 50 nm in diameter, 20 nm in separation, and 150 nm in height can be as high as 80%. The simulation results provide practical clues to the optimum design and fabrication of fiber-optic photoacoustic generators.

ACKNOWLEDGMENT

REFERENCES

1. Sposito, G., C. Ward, P. Cawley, P. B. Nagy, and C. Scruby, "A review of non-destructive techniques for the detection of creep damage in power plant steels," *NDT & E Int.*, Vol. 43, No. 7, 555–567, 2010.

2. Harrison, T., J. C. Ranasinghesagara, H. Lu, K. Mathewson, A. Walsh, and R. J. Zemp, "Combined photoacoustic and ultrasound biomicroscopy," *Opt. Express*, Vol. 17, No. 24, 22041–22046, 2009.

3. Foster, F. S., J. Mehi, M. Lukacs, D. Hirson, C. White, C. Chaggares, and A. Needles, "A new 15–50 MHz array-based micro-ultrasound scanner for preclinical imaging," *Ultrasound Med. Biol.*, Vol. 35, No. 10, 1700–1708, 2009.

4. Fomitchov, P. A., A. K. Kromine, and S. Krishnaswamy, "Photoacoustic probes for nondestructive testing and biomedical applications," *Appl. Opt.*, Vol. 41, No. 22, 4451–4459, 2002.

5. Hou, Y., J.-S. Kim, S.-W. Huang, S. Ashkenazi, L. J. Guo, and M. O'Donnell, "Characterization of a broadband all-optical ultrasound transducer-from optical and acoustical properties to imaging," *IEEE Trans. Ultrason., Ferroelectr., Freq. Control.*, Vol. 55, No. 8, 1867–1877, 2008.

6. Biagi, E., F. Margheri, and D. Menichelli, "Efficient laser-ultrasound generation by using heavily absorbing films as targets," *IEEE Trans. Ultrason., Ferroelectr., Freq. Control.*, Vol. 48, No. 6, 1669–1680, 2001.

7. Hou, Y., J.-S. Kim, S. Ashkenazi, M. O'Donnell, and L. J. Guo, "Optical generation of high frequency ultrasound using two-

dimensional gold nanostructure," *Appl. Phys. Lett.*, Vol. 89, No. 9, 093901, 2006.

8. Tian, Y., N. Wu, K. Sun, X. Zou, and X. Wang, "Numerical simulation of fiber-optic photoacoustic generator using nanocomposite materials," *J. Comput. Acoust.*, Vol. 21, No. 2, 1350002, 2013.

9. Hou, Y., J.-S. Kim, S. Ashkenazi, S.-W. Huang, L. J. Guo, and M. O'Donnell, "Broadband all-optical ultrasound transducers," *Appl. Phys. Lett.*, Vol. 91, No. 7, 073507, 2007.

10. Jain, P. K., K. S. Lee, I. H. El-Sayed, and M. A. El-Sayed, "Calculated absorption and scattering properties of gold nanoparticles of different size, shape, and composition: Applications in biological imaging and biomedicine," *J. Phys. Chem. B.*, Vol. 110, No. 14, 7238–7248, 2006.

11. Yang, X., E. W. Stein, S. Ashkenazi, and L. V. Wang, "Nanoparticles for photoacoustic imaging," *Wiley Interdiscip. Rev. Nanomed. Nanobiotechnol.*, Vol. 1, No. 4, 360–368, 2009.

12. Wu, N., Y. Tian, X. Zou, V. Silva, A. Chery, and X. Wang, "High-efficiency optical ultrasound generation using one-pot synthesized polydimethylsiloxane-gold nanoparticle nanocomposite," *J. Opt. Soc. Am. B*, Vol. 29, No. 8, 2016–2020, 2012.

13. Gong, Y., K. Li, J. Huang, N. J. Copner, A. Davies, L. Wang, and T. Duan, "Frequency-selective nanostructured plasmonic absorber by highly lossy interface mode," *Progress In Electromagnetics Research*, Vol. 124, 511–525, 2012.

14. Temple, T. L. and D. M. Bagnall, "Optical properties of gold and aluminium nanoparticles for silicon solar cell applications," *J. Appl. Phys.*, Vol. 109, No. 8, 084343, 2011.

15. Nguyen, H., F. Sidiroglou, S. F. Collins, G. W. Baxter, A. Roberts, and T. J. Davis, "Periodic array of nanoholes on gold-coated optical fiber end-faces for surface plasmon resonance liquid refractive index sensing," *Proc. SPIE*, Vol. 8351, 835128, 2012.

16. Tian, Y., N. Wu, X. Zou, H. Felemban, C. Cao, and X. Wang, "Fiber-optic ultrasound generator using periodic gold nanopores fabricated by a focused ion beam," *Opt. Eng.*, Vol. 52, No. 6, 065005, 2013.

17. Mie, G., "Contributions of the optics of turbid media, particularly of colloidal metal solutions," *Ann. Phys.*, Vol. 25, No. 3, 377–445, 1908.

18. Bohren, C. F. and D. R. Huffman, *Absorption and Scattering of Light by Small Particles*, Wiley Interscience, New York, 1983B.

19. Handapangoda, C. C., M. Premaratne, and P. N. Pathirana,

"Plane wave scattering by a spherical dielectric particle in motion: A relativistic extension of the mie theory," *Progress In Electromagnetics Research*, Vol. 112, 349–379, 2011.

20. Draine, B. T. and P. J. Flatau, "Discrete-dipole approximation for scattering calculations," *J. Opt. Soc. Am. A*, Vol. 11, No. 4, 1491–1499, 1994.

21. Kim, S., Y. Jung, G. H. Gu, J. S. Suh, S. M. Park, and S. Ryu, "Discrete dipole approximation calculations of optical properties of silver nanorod arrays in porous anodic alumina," *J. Phys. Chem. C.*, Vol. 113, No. 37, 16321–16328, 2009.

22. Kane, Y., "Numerical solution of initial boundary value problems involving Maxwell's equations in isotropic media," *IEEE T. Antenn. Propag.*, Vol. 14, No. 3, 302–307, 1966.

23. Jiang, H., J. Sabarinathan, T. Manifar, and S. Mittler, "3-D FDTD analysis of gold-nanoparticle-based photonic crystal on slab waveguide," *J. Lightwave Technol.*, Vol. 27, No. 13, 2264–2270, 2009.

24. Weiland, T., "Time domain electromagnetic field computation with finite difference methods," *Int. J. Numer. Model. El.*, Vol. 9, No. 4, 295–319, 1996.

25. Wang, Z. B., B. S. Luk'yanchuk, W. Guo, S. P. Edwardson, D. J. Whitehead, L. Li, Z. Liu, and K. G. Watkins, "The influences of particle number on hot spots in strongly coupled metal nanoparticles chain," *J. Chem. Phys.*, Vol. 128, No. 9, 094705-5, 2008.

26. Johnson, P. B. and R. W. Christy, "Optical constants of noble metals," *Phys. Rev. B*, Vol. 6, No. 12, 4370–4379, 1972.

27. Shulz, L. G., "The optical constants of silver, gold, copper and aluminum. I. The absorption coefficient k. And II. the index of refraction n," *J. Opt. Soc. Am. A*, Vol. 44, No. 5, 357–362, 362–367, 1954.

28. Ordal, M. A., L. L. Long, R. J. Bell, S. E. Bell, R. W. Alexander, Jr., and C. A. Ward, "Optical properties of the metals Al, Co, Cu, Au, Fe, Pb, Ni, Pd, Pt, Ag, Ti, and W in the infrared and far infrared," *Appl. Opt.* , Vol. 22, No. 7, 1099–1119, 1983.

29. CST Microwave Studio 2010, (http://www.cst.com/Content/Products/MWS/Overview.aspx).